Model Based Research on ICE Engine Powered by Alternative Fuels

Adrian Chmielewski, Robert Gumiński, Tomasz Mydłowski, Artur Małecki and Krzysztof Bogdziński

Abstract The paper presents 2 DOF dynamic model of the piston-crankshaft system of HONDA NHX 110. The piston-crankshaft system was combined with pressure curve, which was obtained from the experimental research, measured in the cylinder during the execution of the working cycle of ICE engine. In the article the theoretical and analytical dependencies, which described heat generation in the cylinder, have been presented. Based on research results obtained from the experiment and simulation model the value of angular displacement, velocity and acceleration value of flywheel and shaft have been illustrated. Moreover piston displacement, velocity and acceleration has been showed. In the paper, the research results and simulation results at different angles of the ignition advance of ICE engine powered by compressed natural gas—CNG have been analyzed and compared.

Keywords 2 DOF dynamic model · ICE engine · Alternative fuels
Piston-crankshaft system

A. Chmielewski (✉) · R. Gumiński · T. Mydłowski · A. Małecki · K. Bogdziński
Faculty of Automotive and Construction Machinery Engineering, Institute of Vehicles, Warsaw University of Technology, Narbutta 84, 02–524 Warsaw, Poland
e-mail: a.chmielewski@mechatronika.net.pl

R. Gumiński
e-mail: rgumin@simr.pw.edu.pl

T. Mydłowski
e-mail: mydlowski@mechatronika.net.pl

A. Małecki
e-mail: a.malecki85@gmail.com

K. Bogdziński
e-mail: k.bogdzinski@mechatronika.net.pl

J. Awrejcewicz (ed.), *Dynamical Systems in Applications*,
Springer Proceedings in Mathematics & Statistics 249,
https://doi.org/10.1007/978-3-319-96601-4_4

1 Introduction

Nowadays more and more attention is given to distributed energy generation systems [1, 2], which include: renewable energy sources or cogeneration systems [3–6]. Some of them including internal combustion engines (ICE) powered by alternative fuels (e.g. biogas) [7, 8]. Especially important from economic stand point are low power output engines.

The structure of the following work is as follows: in Sect. 2 a research stand for conducting pressure change measurements inside the combustion chamber of a CNG powered ICE was presented. In Sect. 3 presents an analytical description of piston and crankshaft system and description of heat exchange in combustion chamber. Results of the research were used in a model simulation (model of the piston and crankshaft mechanism of low power output Honda NHX internal combustion engine powered by CNG with 2 degrees of freedom was used). Analytical dependencies of the model are presented in Sect. 3. In Sect. 4 the simulation model and simulation results are presented. Section 5 contains the main conclusions and limitations of usage of simulation models for describing thermodynamic processes.

2 Test Stand Description

The engine test stand, presented in Fig. 1, consisted of the Honda NHX 110 4 stroke internal combustion engine, an electric machine, the programmable engine management unit ECU MASTER EMU, the measurement track and control system. The engine was equipped with the trifunctional catalytic converter. The receiver of the generated torque was a brushless electric motor with permanent magnets, working as an electric generator. The power receiving circuit consisted of a 3-phase rectifying bridge (maximum voltage: 400 V, maximum current: 300 A), a transistor module, a resistor module (0.05 Ω), a brushless electric motor with permanent magnets (resistance: 0.0004 Ω, input voltage: 30–70 V, rotational speed: 150 rpm per 1 V of voltage input, maximum rotational speed 10,500 rpm, current draw with no load: 13 A at 20 V voltage input). Control over the transistor module was performed by a custom microprocessor control module, described in detail in [6, 9–11]. A toothed belt transmission (ratio $i = 1.42$) was used to transfer the torque from engine crankshaft to the electric generator. Torque was measured with a Zemic L6N load cell sensor (accuracy class: C3). Engine crankshaft angle was registered with a single-turn digital absolute encoder with 14 bit precision. The SSI standard communication protocol was used for data transmission from the encoder, at a rate of 44.9 kHz, which resulted in accuracy of 0.5° CA (crankshaft angle) at 3800 rpm (1° CA at 7600 rpm respectively). Detailed description of the test stand was provided in [8, 9].

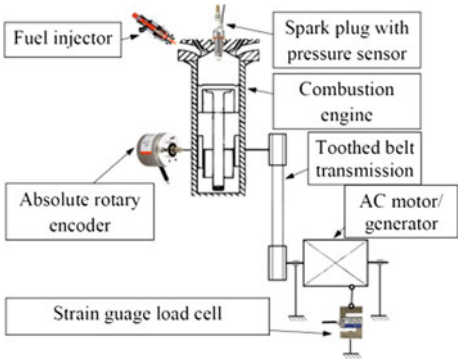

Fig. 1 The scheme of the test stand

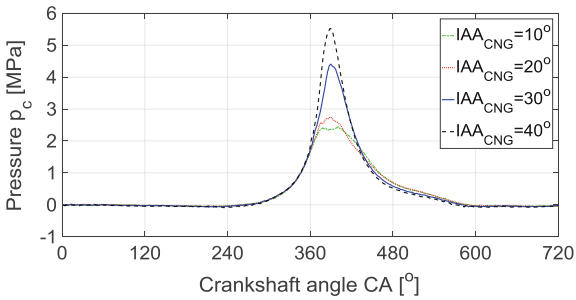

Fig. 2 Open indicator graphs for ICE powered by CNG

2.1 Research Results—Indicator Pressure Graphs

In the following section, open indicator graphs obtained from experimental research are presented (Fig. 2). Results for ICE powered by CNG.

Analysis of Fig. 2 shows that with the increase of ignition advance angle, the maximum pressure in the combustion chamber increases (for ignition advance angle from ranging from 0 to 720 CA). The obtained results of pressure change were used as source data for the piston and crankshaft assembly with 2 degrees of freedom model of Honda NHX 110 engine, presented in Sect. 2.

3 Analytical Background

3.1 Analytical Description of 2DOF Crankshaft Assembly

In the following section the analytical dependencies of the crankshaft assembly with 2 degrees of freedom were presented. A geometry model was presented in Fig. 3. The model assumes a static reduction of crankshaft masses. Similar assumptions were made in [12–16]. The analyzed physical model has 2 degrees of freedom. The fragment of the crankshaft connecting the flywheel with the crank has rigidity k.

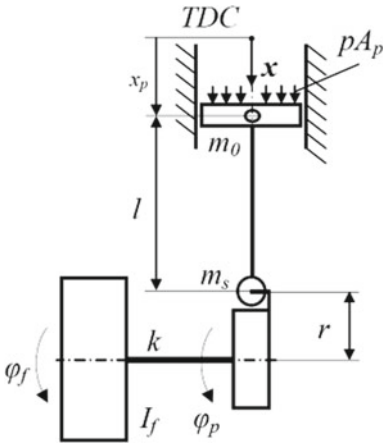

Fig. 3 Diagram of the crankshaft assembly with 2 DOF

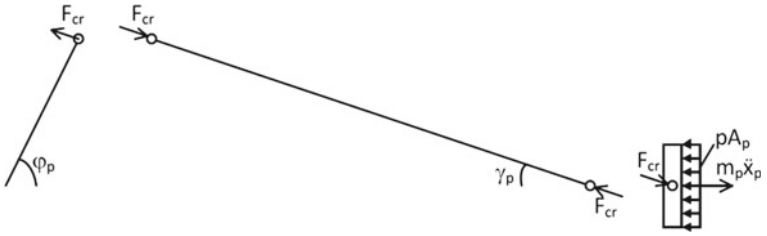

Fig. 4 Diagram presenting the distribution of force and angles in analyzed system

In Fig. 4 a diagram of the crankshaft assembly with indication of forces and torque was presented.

Based on analysis of Figs. 3 and 4, the equation for the moments of inertia of crankshaft's crank can be written:

$$F_{cr} r \sin(\varphi_p + \gamma_p) - I_p \ddot{\varphi}_p - k(\varphi_p - \varphi_f) = 0 \tag{1}$$

and the dependence for sum of moments of the flywheel can be written:

$$I_f \ddot{\varphi}_f - k(\varphi_p - \varphi_f) = 0 \tag{2}$$

The sum of projected forces on x axis for the piston (based on Figs. 3 and 4) is:

$$F_{cr} \cos \gamma_p + m_p \ddot{x}_p - pA_p = 0 \tag{3}$$

From analysis of Fig. 4, knowing that:

$$\frac{l}{\sin\varphi_p} = \frac{r}{\sin\gamma_p} \tag{4}$$

Using the law of sines, the dependencies between γ_p and φ_p can be determined:

$$\cos\gamma_p = \sqrt{1 - \frac{r^2}{l^2}\sin^2\varphi_p} = \sqrt{1 - \lambda^2\sin^2\varphi_p} \tag{5}$$

Fitting the dependencies (2–5) into dependency (1) results in equation for angular acceleration of the piston:

$$\ddot{\varphi}_p = \frac{r\left(pA_p - m_p\ddot{x}_p\right)}{I_p}\frac{\left(\sin\varphi_p\sqrt{1-\lambda^2\sin^2\varphi_p} + \lambda\sin\varphi_p\cos\varphi_p\right)}{\sqrt{1-\lambda^2\sin^2\varphi_p}} - \frac{k}{I_p}(\varphi_p - \varphi_f) \tag{6}$$

From geometrical and trigonometric dependencies the final unknown value can be determined from Eq. (6), linear displacement of piston x_p:

$$x_p = r + l - r\cos\varphi_p - l\cos\gamma_p \tag{7}$$

After transformations, knowing that $\lambda = r/l$:

$$\begin{aligned} x_p &= r\left\{(1-\cos\varphi_p) + \frac{l}{r}(1 - \sqrt{1 - \frac{r^2}{l^2}\sin^2\varphi_p})\right\} \\ &= r\left\{(1-\cos\varphi_p) + \frac{1}{\lambda}(1 - \sqrt{1 - \lambda^2\sin^2\varphi_p})\right\} \end{aligned} \tag{8}$$

The result is:

$$x_p = r\left\{(1-\cos\varphi_p) + \frac{\lambda}{4}(1-\cos 2\varphi_p)\right\} \tag{9}$$

Differentiating the dependency (9) results in dependency for the speed of the piston:

$$\dot{x}_p = \frac{dx_p}{dt} = r\dot{\varphi}_p\left\{\sin\varphi_p + \frac{\lambda}{2}\sin 2\varphi_p\right\} \tag{10}$$

Differentiating for the second time (8) results in dependency for acceleration of the piston:

$$\ddot{x}_p = \frac{d^2x_{p0}}{dt^2} = r\left[\ddot{\varphi}_p\left(\sin\varphi_p + \frac{\lambda}{2}\sin 2\varphi_p\right) + \dot{\varphi}_p^2\left(\cos\varphi_p + \lambda\cos 2\varphi_p\right)\right] \tag{11}$$

Transforming and differentiating the dependency (2) twice results in the equation for angular acceleration of the flywheel:

$$\ddot{\varphi}_f = \frac{k}{I_f}(\varphi_p - \varphi_f) \tag{12}$$

In Eq. (3) one unknown value, p, is present. The value can be determined from the thermodynamic domain, which was analyzed in Sect. 3.2.

3.2 Analytical Dependencies of Thermodynamic Domain

In order to determine the pressure changes inside the combustion chamber with the use of the first law of thermodynamics, using the zero-dimensional model, it can be written that in accordance with the law of conservation of energy (for low power output engine) [17–23]:

$$\begin{aligned}\frac{dQ_h}{d\varphi} &= \frac{c_v}{R}\left(p\frac{dV}{d\varphi} + V_c\frac{dp}{d\varphi}\right) + p\frac{dV_c}{d\varphi} + \frac{dQ_{hetr}}{d\varphi} \\ &= \frac{1}{n-1}\left(p\frac{dV_c}{d\varphi} + V_c\frac{dp}{d\varphi}\right) + p\frac{dV_c}{d\varphi} + \frac{dQ_{hetr}}{d\varphi}\end{aligned} \tag{13}$$

Transforming the dependency (13), $dp/d\varphi$ can be determined:

$$\frac{dp}{d\varphi} = \frac{n-1}{V_c}\left(\frac{dQ_h}{d\varphi} - \frac{dQ_{hetr}}{d\varphi}\right) - \frac{n}{V_c}p\frac{dV_c}{d\varphi} \tag{14}$$

where: n—the ratio of specific heat (−), n =1.338-6 × $10^{-5}T_{gas}$+$10^{-8}T_{gas}^2$, T_{gas}=$pV/m_{air}R$, T_{gas}—the temperature of the flowing gas (K), m_{air}—the mass of the air in the cylinder (kg), R—the individual gas constant (J/kgK).

The rate of heat transfer Q_{hert}/dt from the flowing gas to the combustion chamber wall is dominated by the forced convection [18, 19], so the following can be calculated:

$$\begin{aligned}\frac{dQ_{hert}}{dt} &= hA\left(T_{gas} - T_{spt}\right) = \overbrace{St\varsigma c_p v}^{h} A\left(\frac{pV_c}{m_{air}R} - T_{spt}\right) \\ &= St\varsigma\frac{\overbrace{R}^{c_p}}{1-\frac{1}{n}}vA\left(\frac{pV_c}{m_{air}R} - T_{spt}\right) \\ &= 0.715\exp(-0.14(\dot{x}_{p\,mean}))\varsigma\frac{R}{1-\frac{1}{n}}vA\left(\frac{pV_c}{m_{air}R} - T_{spt}\right)\end{aligned} \tag{15}$$

where: c_p—specific heat (J/kgK), St—the Stanton number (–), v—turbulent gas fluctuating velocity (m/s), v = 0.5 ($\dot{x}_{p\,mean}$), T_{spt}—measured temperature of the spark plug (K).

The heat flux in combustion chamber can be calculated by solving the partial differential equation which contains two boundary conditions:

$$\frac{\partial T}{\partial t} = \alpha \frac{\partial T^2}{\partial^2 x} \left| \begin{array}{l} T(0,t) = T_{win}(t)\ for\ x = 0 \\ T(a,t) = T_{wot}(t)\ for\ x = a \end{array} \right. \tag{16}$$

where: T_{win}—instantaneous temperature inside of the cylinder wall (K), T_{wot}—the steady state temperature of the cylinder of the surface of the outside wall at distance a from the inside wall surface (K), α—thermal conductivity, $\alpha = k/\zeta c$, k—thermal conductivity (W/mK), c—the specific heat (J/kgK), ζ—gas density (kg/m^3).

T_{win} can be calculated as follows [19]:

$$T_{win} = T_{wmean} + \sum_{n=1}^{M} (A_n \cos(n\omega t) + B_n \sin(n\omega t)) \tag{17}$$

where: T_{wmean}—time averaged value of T_{win}, $\omega = \dot{\varphi}_p$—the angular frequency of the temperature variation—the half of the engine angular velocity for the four-stroke engine, M—harmonic number (–).

We can write the following solution of (17):

$$\begin{aligned} T(x,t) &= T_{wmean} - (T_{wmean} - T_{wot}) + \sum_{n=1}^{\infty} (\exp(-c_n x)) E_n(x,t) \\ &= T_{wmean} - (T_{wmean} - T_{wot}) \\ &\quad + \sum_{n=1}^{\infty} (\exp(-c_n x)) \overbrace{A_n \cos(n\dot{\varphi}t - c_n x) + B_n \sin(n\dot{\varphi}t - c_n x)}^{E_n(x,t)} \\ &= T_{wmean} - (T_{wmean} - T_{wot}) \\ &\quad + \sum_{n=1}^{\infty} (\exp(-c_n x)) \overbrace{\frac{2}{\tau} \int_0^{\tau} T_w(t) \cos(\dot{\varphi} n t) dt}^{A_n} \cos(n\dot{\varphi}t - \overbrace{\sqrt{\frac{n\dot{\varphi}}{2\alpha}}}^{c_n} x) \\ &\quad + \overbrace{\frac{2}{\tau} \int_0^{\tau} T_w(t) \cos(\dot{\varphi} n t) dt}^{B_n} \sin(n\dot{\varphi}t - \overbrace{\sqrt{\frac{n\dot{\varphi}}{2\alpha}}}^{c_n} x) \end{aligned} \tag{18}$$

The heat flux at the cylinder (for $x = 0$) can be expressed by using Furier's law as follows:

$$q(t) = -k\left.\frac{\partial T}{\partial x}\right|_{x=0} = \frac{k}{a}(T_{wmean} - T_{wot}) + k\sum_{n=1}^{M} c_n\{([A_n + B_n]\cos(n\dot{\varphi}t) + ([B_n - A_n]\sin(n\dot{\varphi}t)\} \tag{19}$$

The useful formula for small scale engine proposed by Wu-Chen-Hiseh-Ke [18, 19] allows to calculate T_{spt} with use of intake manifold pressure p_{imp}, based on experimental research:

$$T_{spt} = b_{spt1}\omega + b_{spt2}\omega^2 + b_{spt3}p_{imp} + b_{spt4}p_{imp}\omega + b_{spt5}p_{imp}^2 + b_{spt6}\varepsilon \tag{20}$$

where: b_{spi}—coefficients, described in detail in [18, 19] (–), ε—compression ratio (–).

Similarly, we can determine the Stanton number, based on experimental data [18, 19]:

$$St = \psi\varepsilon S^2\left(b\left(10^5 V_c(\varphi)\right)^2 + \exp((l\dot{x}_{mean}^2)\right) \tag{21}$$

where: $\psi\epsilon<5.9;6>$, $l\epsilon<-0.01;\ -0.015>$– coefficients, S—stroke (m), $S = 2r$.

The V_c volume we can calculate to input x_p from (8), we can write as follows:

$$V_c = V_{ch} + Ax_p = \frac{V_{sc}}{\varepsilon - 1} + \frac{\pi d^2}{4}\underbrace{r\left\{(1 - \cos\varphi_p) + \frac{1}{\lambda}(1 - \sqrt{1 - \lambda^2\sin^2\varphi_p})\right\}}_{\mathrm{x_p}}$$

$$= \frac{\overbrace{\frac{\pi d^2}{4}S|_{S=2r}}^{V_{sc}}}{\varepsilon - 1} + \frac{\pi d^2}{4}r\left\{(1 - \cos\varphi_p) + \frac{1}{\lambda}(1 - \sqrt{1 - \lambda^2\sin^2\varphi_p})\right\} \tag{22}$$

The last unknown parameter in (13) and (14) dQ_h. The heat release rate connected with the crank angle can be obtained from the rate of mass fraction calculated as follows:

$$\frac{dQ_h}{d\varphi_p} = w_1\frac{w_2 + 1}{\varphi_{d0}}\left(\frac{\varphi_{\mathrm{deg}} - \varphi_0}{\varphi_{d0}}\right)^{w_2}\exp\left\{-w_1\left(\frac{\varphi_{\mathrm{deg}} - \varphi_0}{\varphi_{d0}}\right)^{w_2+1}\right\}g_f W_u \tag{23}$$

where: w_1=5, w_2=2 according to [18, 19], W_u—the fuel caloric value (MJ/kg), g_f—the fuel mass injected into the cylinder (kg/s), φ_{d0}—the total combustion expressed in crank angle—CA (deg), φ_0—the start of combustion expressed in crank angle—CA (deg), $\varphi_0 = IAA + 25.5p_{\mathrm{in\ manifold}} - 0.0605\dot{\varphi}_p - 0.2801p_{\mathrm{in\ manifold}}\dot{\varphi}_p + 6.88 \times 10^{-4}\dot{\varphi}_p^2$, $p_{inmanifold}$—intake manifold pressure (MPa). The φ_{deg} can be expressed as follows:

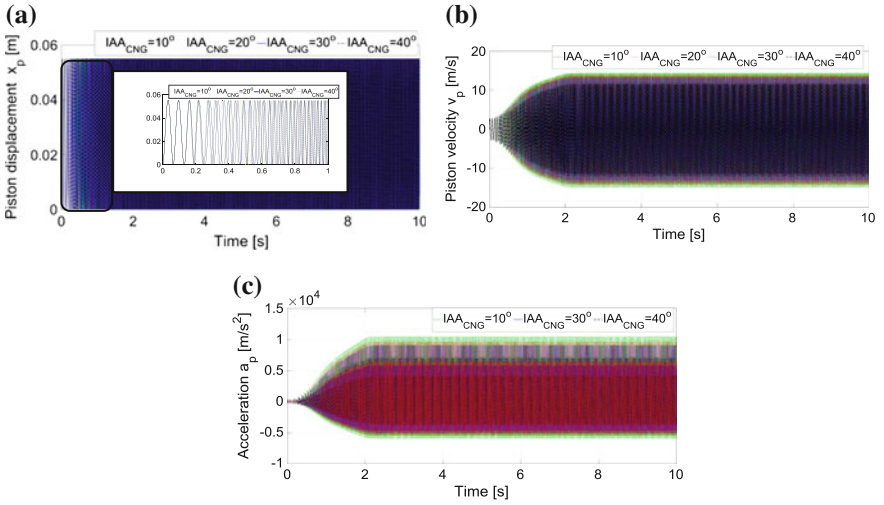

Fig. 5 Parameters of piston of engine fueled by CNG: **a** piston displacement x_p, **b** piston velocity v_p, **c** piston acceleration a_p

$$\varphi_{\text{deg}}[\text{deg}] = \varphi_p[\text{rad}]\frac{180^\circ}{\pi} \tag{24}$$

4 Simulation Model and Simulation Results

A simulation model was prepared based on dependencies (1–12). Changes of pressure were determined and implemented into the model based on analysis of research results presented in Fig. 2, respectively for CNG. Analytical description of pressure changes was presented with use of dependency (13–24).

Figure 5 presents respectively: linear displacement (Fig. 5a), piston velocity (Fig. 5b) and acceleration of the piston (Fig. 5c) of engine fueled by CNG. It presents the results of the simulations for the following main parameters: $k = 9150$ N/m, $l = 0.091$ m, $r = 0.0275$ m, $m_f = 2.851$ kg, $m_p = 0.22$ kg, $r_f = 0.11$ m. Change in rotational speed (Fig. 5a) is caused by change in frequency, the assembly accelerates (up to 2 s), which is shown by the increasing density of displacements. After approximately 2 s (for $IAA_{CNG} = 10$ up to 40 before TDC—Top Dead Centre) the assembly reaches the constant amplitude. If the ignition advance angle IAA_{CNG} increases (which increases the pressure in the cylinder as well) then piston velocity and piston acceleration amplitude decrease. Similar results for the acceleration, velocity, and displacement values have been obtained for the model with 3DOF in the works [12–14]. From a practical point of view, selecting the appropriate inertia of the flywheel I_f is crucial.

Figure 6 presents angular displacement (Fig. 6a), angular velocity (Fig. 6b) and angular acceleration (Fig. 6c) of shaft in engine fueled by CNG. For $IAA_{CNG} = 10$

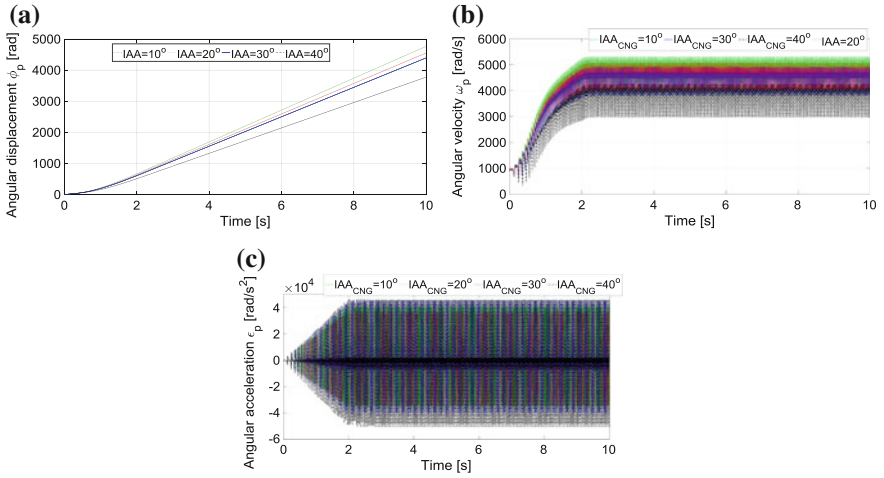

Fig. 6 Parameters of shaft of engine fueled by CNG: **a** angular displacement φ_p, **b** angular velocity ω_p, **c** angular acceleration ε_p

the assembly start up time is the shortest, at 1.95 s, $\omega_{pIAAA\_CNG=10}$=4990 rad/s (Fig. 6b). Angular accelerations in steady state don't exceed 4.2 × 10^4rad/s^2 and −5 × 10^4rad/s^2 for all ignition advance angles.

Figure 7 presents angular displacement (Fig. 7a), speed (Fig. 7b) and acceleration (Fig. 7c) of flywheel of engine fueled by CNG. Greatest increase in angular displacement can be observed in the first second after assembly start up, which accelerates (angular accelerations for all ignition advance angles increase). The highest values of angular accelerations appear for ignition advance angle IAA_{CNG}=40 . This is a result of increased pressure inside the combustion chamber, for IAA_{CNG}=40 p_{max}=5.2 MPa (Fig. 2).As a consequence, greater forces affect the flywheel (visible higher amplitudes of angular speed changes—Fig. 7b).

5 Conclusions

In the article, a model of the piston and crankshaft assembly with 2 degrees of freedom is presented. The model was paired with a chart of indicated pressure changes inside the combustion chamber, acquired from experimental research. To describe the changes of pressure inside the combustion chamber, a zero-dimensional analytical model using the law of conservation of energy was used.

Presented simulations show, that for all ignition advance angles the angular accelerations in steady state do not exceed 4.2 × 10^4rad/s^2 and −5 × 10^4rad/s^2.

The greatest increase in angular displacement can be observed in the first second after assembly start up, as it is accelerating (angular accelerations for all ignition

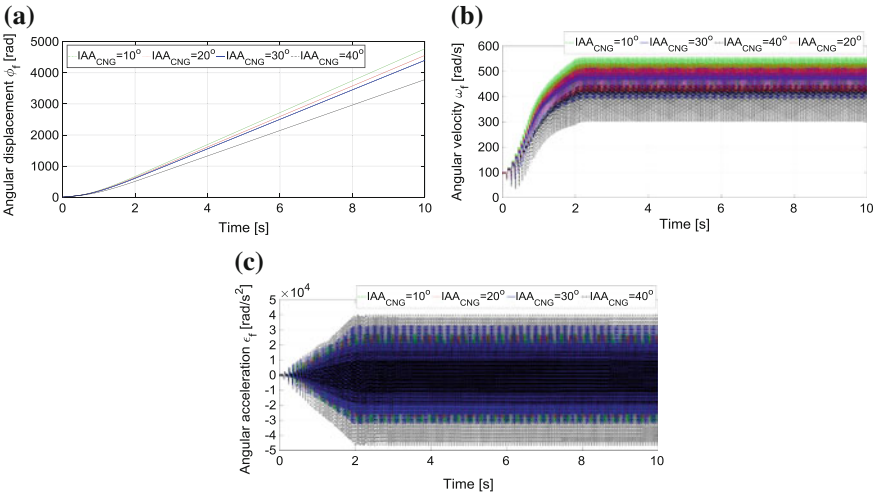

Fig. 7 Parameters of flywheel of engine fueled by CNG: **a** angular displacement φ_f, **b** angular velocity ω_f, **c** angular acceleration ε_f

advance angles increase). The highest values of angular accelerations (Fig. 7c) appear for ignition advance angle $IAA_{CNG} = 40$. This is a result of increased pressure inside the combustion chamber, for $IAA_{CNG} = 40$ $p_{max} = 5.2$ MPa.

The analysis presented in this work and the proposition of merging a piston and crankshaft assembly model with 2 degrees of freedom with a thermodynamic model that takes into account the combustion processes opens up new possibilities of modeling combined systems (mechanical domain—thermodynamic domain).

Below are presented the mechanical equations coupled with equations governing the pressure change.

$$
\begin{cases}
\ddot{\varphi}_p = \dfrac{r\left(pA_p - m_p\ddot{x}_p\right)}{I_p}\dfrac{\left(\sin\varphi_p\sqrt{1-\lambda^2\sin^2\varphi_p} + \lambda\sin\varphi_p\cos\varphi_p\right)}{\sqrt{1-\lambda^2\sin^2\varphi_p}} - \dfrac{k}{I_p}(\varphi_p - \varphi_f) \\
\ddot{\varphi}_f = \dfrac{k}{I_f}(\varphi_p - \varphi_f) \\
\ddot{x}_p = \dfrac{d^2x_{p0}}{dt^2} = r\left[\ddot{\varphi}_p\left(\sin\varphi + \dfrac{\lambda}{2}\sin 2\varphi_p\right) + \dot{\varphi}_p^2\left(\cos\varphi_p + \lambda\cos 2\varphi_p\right)\right] \\
\dfrac{dp}{d\varphi_p} = \dfrac{n-1}{V_c}\left(\dfrac{dQ_h}{d\varphi_p} - \dfrac{dQ_{hetr}}{d\varphi_p}\right) - \dfrac{n}{V_c}p\dfrac{dV_c}{d\varphi_p} \rightarrow p\,(by\,numerical\,solution we\,can\,find\,p) \\
\dfrac{dQ_h}{d\varphi_p} = w_1\dfrac{w_2+1}{\varphi_{d0}}\left(\dfrac{\varphi_{\deg}-\varphi_0}{\varphi_{d0}}\right)^{w_2}\exp\left\{-w_1\left(\dfrac{\varphi_{\deg}-\varphi_0}{\varphi_{d0}}\right)^{w_2+1}\right\}g_f W_u;\ \varphi_{\deg}[\deg] = \varphi[rad]\dfrac{180^o}{\pi} \\
\varphi_0 = IAA + 25.5p_{\text{in manifold}} - 0.0605\dot{\varphi}_p - 0.2801p_{\text{in manifold}}\dot{\varphi}_p + 6.88\times 10^{-4}\dot{\varphi}_p^2 \\
\dfrac{dQ_h}{d\varphi_p} = \dfrac{c_v}{R}\left(p\dfrac{dV_c}{d\varphi_p} + V_c\dfrac{dp}{d\varphi_p}\right) + p\dfrac{dV_c}{d\varphi_p} + \dfrac{dQ_{hetr}}{d\varphi_p} \rightarrow \dfrac{dp}{d\varphi_p}
\end{cases}
$$

$$
\frac{dQ_{hert}}{dt} = hA\left(T_{gas} - T_{spt}\right) = \overbrace{St\varsigma c_p v}^{h}A\left(\frac{pV_c}{m_{air}R} - T_{spt}\right) = St\varsigma\frac{\overbrace{R}^{c_p}}{1-\frac{1}{n}}vA\left(\frac{pV_c}{m_{air}R} - T_{spt}\right) =
$$

$$
0.715\exp(-0.14(\dot{x}_{p\,mean}))\varsigma\frac{R}{1-\frac{1}{n}}vA\left(\frac{pV_c}{m_{air}R} - T_{spt}\right)
$$

$$
V_c = \frac{\overbrace{\frac{\pi d^2}{4}S|_{S=2r}}^{V_{sc}}}{\varepsilon - 1} + \frac{\pi d^2}{4}\overbrace{r\left\{(1-\cos\varphi_p) + \frac{1}{\lambda}(1-\sqrt{1-\lambda^2\sin^2\varphi_p})\right\}}^{x_p} = V_{sc} + \frac{\pi d^2}{4}x_p
$$

$$
\frac{dV_c}{d\varphi_p} = \frac{\pi d^2}{4}\dot{x}_p = \overbrace{r\dot{\varphi}_p\left\{\sin\varphi_p + \frac{\lambda}{2}\sin 2\varphi_p\right\}}^{\dot{x}_p}\frac{\pi d^2}{4}
$$

References

1. Chmielewski, A., Gumiński, R., Mączak, J., Radkowski, S., Szulim, P.: Aspects of balanced development of RES and distributed micro–cogeneration use in Poland: case study of a mCHP with Stirling engine. Renew. Sustain. Energy Rev. **60**, 930–952 (2016)
2. Milewski, J., Szabłowski, Ł., Kuta, J.: Control strategy for an internal combustion engine fuelled by natural gas operating in distributed generation. Energy Procedia **14**, 1478–1483 (2012)
3. Szabłowski, Ł., Milewski, J., Kuta, J., Badyda, K.: Control strategy of a natural gas fuelled piston engine working in distributed generation system. Rynek Energii **3**, 33–40 (2011)
4. Chmielewski, A., Gontarz, S., Gumiński, R., Mączak, J., Szulim, P.: Research study of the micro cogeneration system with automatic loading unit. In: Szewczyk, R., Zieliński, C., Kaliczyńska, M. (eds.) Challenges in Automation, Robotics and Measurement Techniques. Advances in Intelligent Systems and Computing, vol. 440, pp. 375–386. Springer, Cham (2016)
5. Nunes de Faria, M.M., Vargas Machuca Bueno, J.P., Elmas Alami Ayad, S.M.M., Pereira Belchior, C.R.: Thermodynamic simulation model for predicting the performance of spark ignition engines using biogas as fuel. Energy Conversion and Management (2017) (in print)

6. Mydłowski, T., Nader, S., Biskup, K., Jasiński, M.: Wykorzystanie urządzenia ECU Master EMU do sterowania silnikami z zapłonem iskrowym (Using the ECU Master EMU device to control spark ignition combustion engines). Zeszyty Naukowe Instytutu Pojazdów **86**, 125–129 (2011) (in Polish)
7. Małecki, A., Mydłowski, T., Dybała, J.: Badania wpływu zanieczyszczeń biopaliw na sprawność silnika ZI (Research on the impact of biofuels pollutants on the SI engine efficiency). Zeszyty Naukowe Instytutu Pojazdów **99**, 89–97 (2014) (in Polish)
8. Chmielewski, A., Gumiński, R., Mydłowski, T., Małecki, A., Bogdziński, K.: Research study of HONDA NHX 110 powered by an alternative fuel. In: IOP Conference Series: Earth and Environmental Science (EES), Second International Conference on the Sustainable Energy and Environmental Development, SEED 2017 Cracow (in Print)
9. Małecki, A., Mydłowski, T., Dybała, J.: Stanowisko hamowniane do badań silników spalinowych o małych mocach (The engine dynamometer to test internal combustion engines with low power). Zeszyty Naukowe Instytutu Pojazdów **96**, 55–66 (2013) (in Polish)
10. Dybała, J., Mydłowski, T., Małecki, A., Bogdziński, K.: Dynamometer and test stand for low power internal combustion engine. Combust. Engines **162**, 996–1000 (2015)
11. Małecki, A., Mydłowski, T., Radkowski, S.: Przegląd uniwersalnych sterowaników do silników ZI (Review of programmable electronic fuel injection controllers). Zeszyty Naukowe Instytutu Pojazdów **93**, 93–101 (2013)
12. Chmielewski, A., Gumiński, R., Radkowski, S.: Chosen properties of a dynamic model of crankshaft assembly with three degrees of freedom. In: 20th International Conference on Methods and Models in Automation and Robotics 978-1-4799-8701-6/15/$31.00 ©2015 IEEE, pp. 1038–1041 (2015)
13. Chmielewski, A., Gumiński, R., Mączak, J.: Selected properties of the dynamic model of the piston-crankshaft assembly in Stirling engine combined with the thermodynamic submodel. Int. J. Struct. Stab. Dyn. **17**, 1740009 (25 pages) (2017)
14. Chmielewski, A., Gumiński, R., Mączak J., Selected properties of the adiabatic model of the stirling engine combined with the model of the piston-crankshaft system. In: 21st International Conference on Methods and Models in Automation and Robotics (MMAR), 978-1-5090-1866-6/16/$31.00 ©2016 IEEE, pp. 543–548 (2016)
15. Awrejcewicz, J., Kudra, G.: The triple pendulum with barriers and the Piston—connecting rod—cranckshaft model. J. Theor. Appl. Mech. **1**(45), 15–23 (2007)
16. Kudra, G., Awrejcewicz, J.: Modeling and numerical investigation of non-linear dynamics of a mono-cylinder combustion engine. IN: Proceedings of DETC'03 ASME 2003 Design Engineering Technical Conferences and Computers and Information in Engineering Conference, Chicago, Illinois, USA, pp. 1–9 (2003)
17. Pham, P.X., Vo, D.Q., Jazar, R.N.: Development of fuel metering techniques for spark ignition engines. Fuel **206**, 701–715 (2017)
18. Wu, Y.Y., Chen, B.-C., Hsieh, F.C.: Heat transfer model for small-scale air-cooled spark-ignition four-stroke engines. Int. J. Heat Mass Transf. **49**, 3895–3905 (2006)
19. Wu, Y.Y., Chen, B.C., Hsieh, F.C., Ke, C.T.: Heat transfer model for small-scale spark-ignition engines. Int. J. Heat Mass Transf. **52**, 1875–1886 (2009)
20. Morrone, P., Algieri, A., Bova, S.: Development of a lumped model for the characterization of the intake phase in spark-ignition internal combustion engines. Energy Procedia **101**, 590–597 (2016)
21. Nunes, M.M., Vargas Machuca Bueno, J.P., ElmassalamiAyad, S.M.M., Belchior, C.R.P.: Thermodynamic simulation model for predicting the performance of spark ignition engines using biogas fuel. Energy Convers. Manage. **149**, 1096–1108 (2017)
22. Chaudhari, A.J., Sahoo, N., Kulkarni, V.: Simulation models for spark ignition engine: a comparative performance study. Energy Procedia **54**, 330–341 (2014)
23. Chen, B.C., Wu, Y.Y., Hsieh, F.C.: Estimation of engine rotational dynamics using Kalman filter based on a kinematic model. IEEE Trans. Veh. Technol. **8**(59), 3728–3735 (2010)